ORIGINAL RESEARCH ARTICLE

Influence of Globularization Process on Local Texture Evolution of a Near-α Titanium Alloy with a Transformed Microstructure

Z.B. ZHAO, B.H. ZHANG, H. SUN, Q.J. WANG, J.R. LIU, and R. YANG

The microstructure and texture evolution of Ti60 (Ti–5.6Al–3.7Sn–3.2Zr–0.5Mo–0.4Nb–1.0-Ta–0.37Si–0.05C) titanium alloy at two deformation temperatures in the $\alpha + \beta$ two-phase field, 900 °C and 980 °C, have been investigated in this work. The purpose is to elucidate local texture evolution during $\alpha + \beta$ hot working process and the mechanisms by which the macrozones formed for bimodal microstructure. To this end, a lamellar Ti60 ingot was compressed and annealed in the $\alpha + \beta$ phase field. The key finding was that the globularization mechanism of α lamellae and crystallographic orientation evolution of both α and β phases strongly depended on deformation temperature. The experimental findings and analyses suggest that hot working in the low $\alpha + \beta$ two-phase field is beneficial to reducing texture intensity and eliminating the macrozones of near-α titanium alloys.

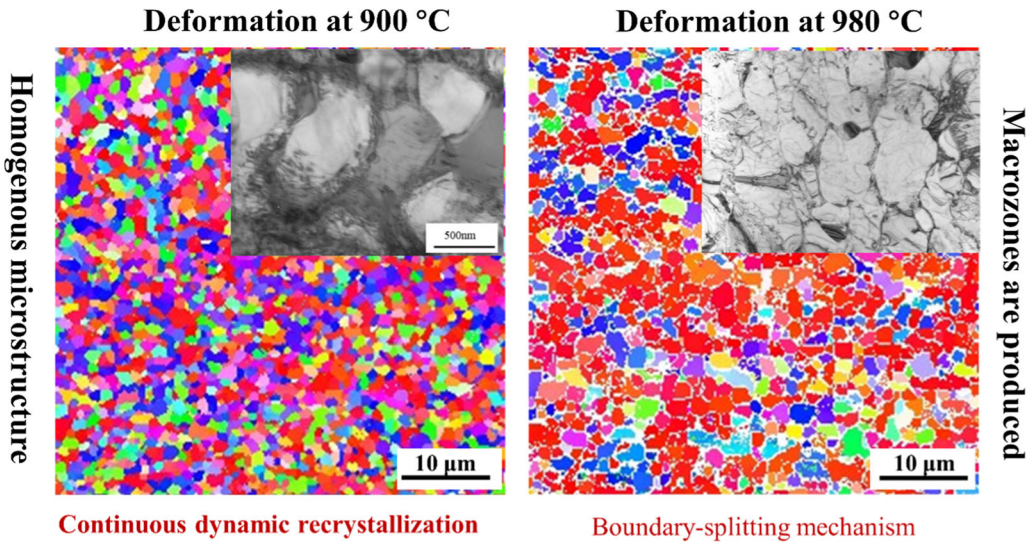

https://doi.org/10.1007/s11661-023-07063-3

I. INTRODUCTION

THE desired microstructure for near-α titanium high-pressure compressor disks of advanced gas turbine engines is often of fine bimodal type.[1–3] In general, bimodal microstructure is obtained by successive deformation steps in the β and $\alpha + \beta$ phase fields,[4,5] and many attempts have been made to obtain a homogenous microstructure by optimizing the process window.[6]

Owing to the great technological importance, the globularization process, which converts the transformed microstructure into an equiaxed one, has been widely studied[7–10] (in this paper the term globularization is

Z.B. ZHAO, H. SUN, Q.J. WANG, J.R. LIU, and R. YANG are with the Shi-Changxu Innovation Center for Advanced Materials, Institute of Metal Research, Chinese Academy of Science, Shenyang 110016, P.R. China. Contact e-mails: zbzhao@imr.ac.cn; qjwang@imr.ac.cn B.H. ZHANG is with the Shi-Changxu Innovation Center for Advanced Materials, Institute of Metal Research, Chinese Academy of Science and also with the School of Materials Science and Engineering, University of Science and Technology of China, Shenyang 110016, P.R. China.

Manuscript submitted August 10, 2022; accepted April 3, 2023.
Article published online May 16, 2023

used in its general sense; globularization and recrystallization are not regarded as mutually exclusive processes). A phase boundary grooving mechanism was proposed by Wiess *et al*. to describe the globularization process of Ti–6Al–4V alloy.[11] They suggested that the α/α boundaries were formed either by intense local shear or dynamic recovery/recrystallization during deformation across individual α lamellae, and the β phase subsequently penetrated the boundary *via* diffusion. They also demonstrated that both high- and low-angle α/α boundaries were formed during the break-up of lamellar α. An interesting recent investigation showed that the globularization process of Ti–6Al–4V at warm temperatures produced a finer microstructure than at hot deformation temperatures. Zherebtsov *et al*. suggested that this globularization process of the α lamellae was accompanied by continuous dynamic recrystallization, and this process occurred in the absence of β phase participation at relatively low temperature.[12]

However, titanium alloys that are homogenous in terms of microstructure morphology can be inhomogeneous in local orientation distribution.[1,2,13–15] Regions of sharp local texture, called 'macrozones,' have been observed in many forging products. A macrozone always corresponds to a region where the β phase always keeps the Burgers orientation relationship (BOR) with the surrounding α_p grains.[1,2,8] As a result, the secondary α laths that have a common *c*-axis with the surrounding α_p grains are preferentially formed by variant selection during $\beta \rightarrow \alpha$ transformation.[8] These macrozones were reported to drastically reduce the fatigue resistance at ambient temperatures of titanium alloys.[16–19] Thus, the orientation distribution of α_p/β grains is a critical aspect influencing the quality of bimodal microstructure of titanium alloys.

Previous studies have concluded that the $\alpha + \beta$ processing plays a major role in formation of macrozones in titanium alloys with a bimodal microstructure.[1,2,8,14] For instance, Behrang Poorganji *et al*. investigated the role of initial structure on microstructure evolution of Ti–1.5Fe alloy in the $\alpha + \beta$ deformation, and found that a finer initial microstructure (in terms of both colony size and interlamellar spacing) by increasing cooling rate is beneficial for the occurrence of dynamic recrystallization and the elimination/reduction of macrozones.[20] The microstructure and texture evolution of Ti6242S alloy bar with equiaxed microstructure was also studied, which revealed the development of the $\langle 11\text{-}20\rangle$//AD (associated with the activated prismatic $\langle a\rangle$ slip of α phase) and $\langle 20\text{-}23\rangle$//AD texture (associated with DRX of α_p phase).[21] To date, numerous investigators have examined the break-up of the lamellar microstructures and studied the globularization mechanisms in titanium alloys; some data suggested that the globularization process of α lamellae may produce a few new α orientations and the equiaxed α grains evolved from an α colony may retain the common *c*-axis during the hot working process.[1,8] The crystallographic orientation evolution of the α phase during hot working is therefore still not well understood. Additionally, some investigators suggested that the α phase has a significant effect on the β phase evolution.[22,23] Because the β phase is scanty in near α titanium alloys it is hard to detect after deformation and this increases the difficulty to elucidate the role of the β phase in the macrozone formation.

The improvement of the dwell fatigue life depends on minimizing or even eliminating the occurrence of macrozones during hot working in forged products. The aim of this work is to study the effect of deformation temperature on the microstructure and crystallographic orientation evolution in a near α alloy with fully lamellar starting microstructure. For this purpose, compressive tests were conducted at low (900 °C) and medial (980 °C) temperatures of the $\alpha + \beta$ phase field of Ti60 titanium alloy, and the microstructure and orientation evolution were analyzed.

II. EXPERIMENTAL

The as-received material is a Ti60 bar forged in its $\alpha + \beta$ phase field to a diameter of 45 mm. The measured composition by the titration method in weight percentage is 5.6 pct Al, 3.7 pct Sn, 3.2 pct Zr, 0.5 pct Mo, 0.4 pct Nb, 1.0 pct Ta, 0.37 pct Si, and 0.05 pct C, balanced by Ti. The β transus of this bar is determined as approximately 1040 °C by the metallographic method. The bar was forged and annealed in the $\alpha + \beta$ two-phase field followed by air cooling to achieve a fine bimodal microstructure. This bar was finally heated at 1070 °C for 1 hour followed by air cooling (AC) to produce a fully lamellar microstructure (Figure 1). The microstructure consisted of large α lamellar colonies formed within prior β grains, with the lamella thickness measured to be 3.4 ± 0.24 μm and the maximum α colony size being around 700 μm. The texture of the α phase is presented later in Figure 3(a). The size of the prior β grains is approximately 2.0 ± 0.31 mm and the volume fraction of β retained at the α lamella boundaries was estimated to be 5 ± 0.4 pct.

Cylindrical samples of length 40 mm and diameter 30 mm were machined from the β-annealed Ti60 bar. All samples were covered by asbestos and heated at deformation temperatures for 1 hour to ensure uniform

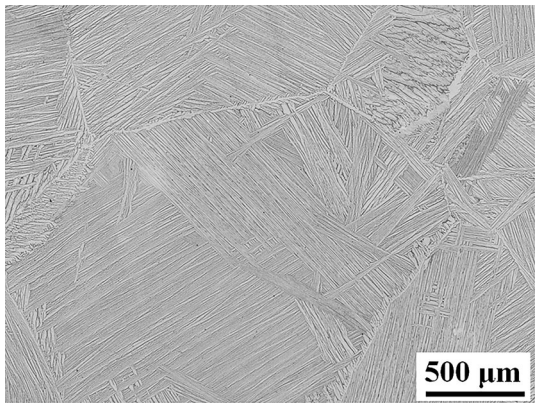

Fig. 1—Microstructure of Ti60 bar after heat treatment at 1070 °C, 1 h/AC.

temperature distribution. Trial compression tests were conducted at temperatures ranging from 860 °C to 1020 °C and the deformed microstructures were observed. Based on these preliminary experiments, the deformation temperatures of 900 °C and 980 °C were selected to represent deformation in the low and medial $\alpha + \beta$ two-phase field, respectively. The equilibrium volume fraction of the β phase at these two temperatures were estimated to be 9 and 30 pct, respectively, and the 1 hour holding at temperature prior to compression is thought to be sufficient for the β phase to attain its equilibrium amount. The samples were compressed at a velocity of approximately 8 mm/s to height reductions of 25, 50, and 70 pct. We chose this deformation velocity because it is similar to that experienced by a Ti60 forged disk; conversion to strain rate was not made because the laboratory compression machine we used did not have this option. The compression direction (CD) of the specimens was always parallel to the axial direction (AD) of the original bar. The samples were water-quenched after the compression. To obtain bimodal microstructure, some samples were annealed at 1020 °C for 2 hours followed by air cooling.

All specimens were taken from the central (maximum deformation) region of the deformed samples for microstructure determination using a Nano SEM430 scanning electron microscope (SEM) equipped with a Channel 5 system and a FEI/Nova transmission electron microscope (TEM). Laboratory X-ray texture measurements with a 5 mm × 5 mm beam were made on each sample covering approximately 120 colonies and thus were considered representative of bulk material. Electron backscatter diffraction (EBSD) orientation data, in contrast, were obtained from only a few colonies and were used to characterize local texture and orientation variation. To obtain more information on the texture of the material, the α_p grains were separated from secondary α laths by contrasting the morphological difference between equiaxed α_p grains and secondary α laths in optical images captured from the corresponding EBSD scanning areas. Meanwhile, the prior β orientation maps were also calculated from the secondary α orientation according to Burgers orientation relationship.

III. RESULTS

A. *Microstructure After Globularization*

The as-deformed microstructures at both 900 °C and 980 °C are shown in Figure 2. The main morphological feature of microstructure evolution is α lamellae rotation toward the radial direction (RD), so that the lamellar boundaries become perpendicular to the compression axis, during deformation. Dynamic globularization of α lamellae occurs with the increase in strain. During deformation at 900 °C, some kinking occurred to the α lamellae (*e.g.*, circled areas in Figure 2(a)) that were approximately parallel to the compression axis at a height reduction of 25 pct (Figure 2(a)). Colonies with lamellar boundaries initially almost parallel to the RD showed little morphological change and globularization had not yet begun at such a low strain level. With an increase in strain to the height reduction of 50 pct (Figure 2(c)), all α lamellae rotated to RD and the difference between the colonies gradually disappeared due to spheroidization. At a height reduction of 70 pct (Figure 2(e)), no trace of original lamellar boundaries could be seen and the lamellae were completely broken-up with an α grain size of 1.5 to 2 μm.

At the deformation temperature of 980 °C, the characteristics of microstructure evolution are different. The dynamic spheroidization of the α phase becomes easier than at 900 °C. A few equiaxed α grains formed already at 25 pct height reduction (Figure 2(b)). The discrepancy of the microstructure at height reductions of 50 and 70 pct is small as shown in Figures 3(d) and (f). In both cases the lamellae were almost completely globularized with an α grain size of 3 to 4 μm, although the traces of original lamellae could still be seen on the low-magnification image.

The texture evolution of α phase is shown in Figure 3. The starting material had strong and complex texture components in the {0001} pole figure (Figure 3(a)). The main texture component consisted of c-axes that were concentrated around the AD with a maximum intensity of 12 times random intensity. Some c-axes were also distributed around a number of radial directions (RDs). The {11-20} pole figure did not exhibit very obvious concentrations. The α texture had completely changed after globularization: At 900 °C, the texture was found to be weak with 70 pct height reduction (Figure 3(b)). By contrast as shown in Figure 3(c), a high density $\langle 11\text{-}20 \rangle$//AD fiber texture with the c-axes spreading around different RDs was obtained after dynamic globularization at 980 °C.

EBSD analysis was conducted to characterize crystallographic orientation evolution accompanying the globularization process. The local texture characteristics after deformation and globularization at 980 °C are significantly different from that deformed at 900 °C. At 900 °C, a complete equiaxed microstructure with homogenous local orientation distribution was obtained (Figure 4(a)). Contrastively, microstructure featuring a very strong local texture (Figure 4(b)) was produced after deformation at 980 °C.

IV. ANALYSIS

Changes in the morphology and texture of α phase are closely related to changing deformation process, as well as globularization mechanism during compression. For lamellar microstructure with compression in the $\alpha + \beta$ phase field, the main deformation mechanisms comprise the slip and rotation of the α lamellae toward the metal flow directions.[12,24] While in a few others, localized shearing occurred to those α lamellae that were approximately parallel to the compression axis,[11,12,24] and fragmented α grains with random orientation are formed in local shear zones.[24] In fact, even though fragmentation and globularization of the α phase is difficult to discern in morphology, the fragmentation is

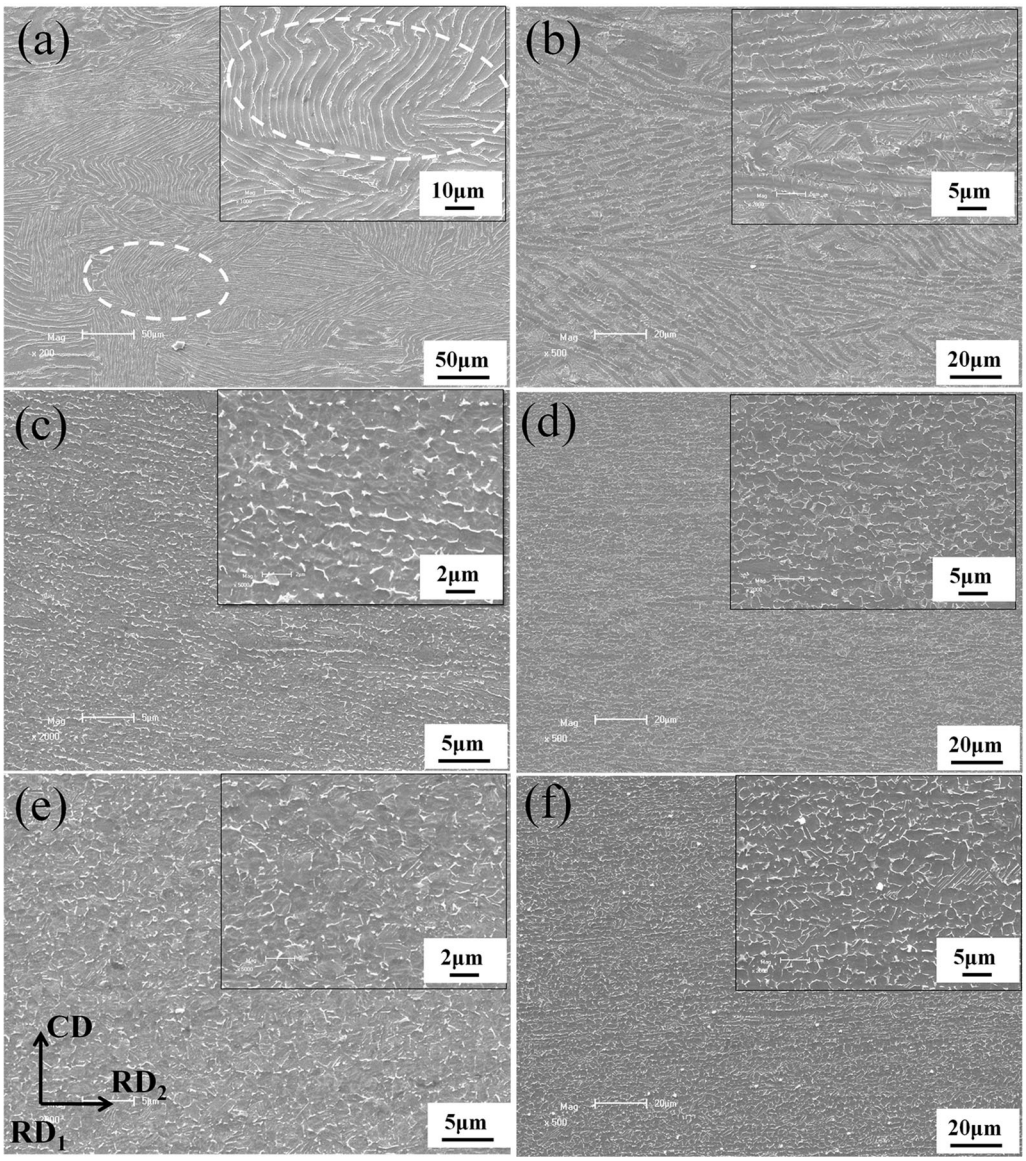

Fig. 2—SEM images of Ti60 alloy after height reductions of (*a*) and (*b*) 25 pct, (*c*) and (*d*) 50 pct and (*e*) and (*f*) 70 pct by compression at (a), (c) and (e) 900 °C and (b), (d) and (f) 980 °C. The compression axis is vertical. Magnified images are shown as insets.

rather sporadic and thus cannot be considered as the main mechanism of microstructure evolution for the α phase.

The main difference between compressing the Ti60 alloy at either 900 °C or 980 °C is the ratio between the α and β phases. At 900 °C, one might assume that the deformation is mainly accommodated by the α phase. It can be deduced that decreasing the deformation temperature during the α + β phase field promotes the orientation gradient by increasing the slip within the α lath and muti-slip activity, which results in the formation of a fine subgrain structure. At 980 °C, deformation was mainly accommodated by the β phase which having lower flow stress,[25] and the α lath evolved in a manner similar to a hard lamellar within a soft matrix. In this case, less slip within the α lath was occur.

In the α phase, the texture development accompanying the globularization process is caused by deformation. The operating slip systems in α titanium during plastic deformation include basal $\langle a \rangle$, pyramidal$\langle a \rangle$, pyramidal $\langle a + c \rangle$, and prismatic$\langle a \rangle$.[26–29] The critical resolved shear stress ratios of prismatic$\langle a \rangle$-to-other slip systems seems to increase with temperature, and it is commonly accepted that the prismatic $\langle a \rangle$ slip is the dominant deformation mode, even at elevated temperatures.[24,30,31] Meanwhile, the relative quantity of the easiest slip mode (*i.e.*, prismatic $\langle a \rangle$ slip) tends to increase in such a soft β matrix.[32] Analysis of the active slip mode of this work also revealed the prismatic $\langle a \rangle$ slip was always the most easily activated slip system at both temperatures.[33] As a result, the preferentially activated prismatic plane normally rotates toward the compression axis with strain. Because the Schmid factor of the prismatic $\langle a \rangle$ slip increases with the increasing angle between the deformation direction and crystallographic *c*-axis,[34] it also

could be deduced that the grains would become more deformable when the deformation was supported by prismatic $\langle a \rangle$ slip as the strain increased.

The rotation of the α lamellae also has a similar effect, that is, the *c*-axis tends to align with the metal flow direction, due to the broad face of the α lamellae, which is nearly parallel to its crystallographic *c*-axis in titanium alloys.[35–38]

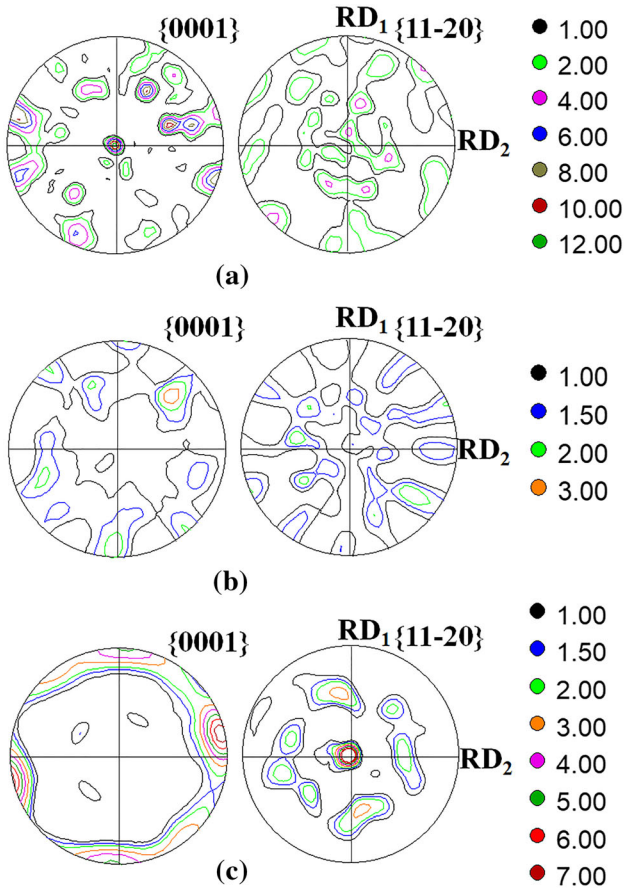

Fig. 3—α texture represented by {0001} and {11-20} pole figures measured by XRD, of (*a*) the initial microstructure and after 70 pct deformation at (*b*) 900 °C and (*c*) 980 °C.

Assuming for a moment that the slips in the α phase and rotation of the α lath do control the α texture's evolution, the deformation texture component should be similar for 900 °C and 980 °C deformed samples, that is the crystallographic *c*-axes of α phase spreading around different RDs of the sample. This is inconsistent with the experimental results. After compression at 900 °C, a microstructure with a homogenous distribution, in terms of crystallographic orientation, is obtained, as shown in Figure 3(b). After compression at 980 °C, a microstructure with a strong texture is produced, as shown in Figure 3(c). Additionally, the local texture distribution also showing significant differences when comparing 900 °C deformed sample and 980 °C deformed sample as shown in Figure 4.

The differences of the two microstructures shown in Figures 2 through 4 probably indicate the largest possible effect of temperature on globularization process of α lamella in Ti60 alloy. To verify these speculates and straightly put forward the microstructure evolution process, TEM and EBSD analyses were carried out. It could be assumed that the dislocation density was low in the undeformed α laths, and it increased significantly after a height reduction of 25 pct at 900 °C (Figure 5(a)). Dislocation walls/pile-ups and cell substructures were observed in some of the laths. For a few α laths, the original α/β boundaries disappeared (such as in the region marked by a rectangle in Figure 5(a)) and some equiaxed α subgrains/grains with sizes of 300 to 700 nm were formed (see Figures 5(a) and (b)) although the equiaxed α grains are still too small to be observed under SEM. At height reduction of 50 (Figure 5(c)) and of 70 pct (Figure 5(d)), the microstructure was remarkably changed: An equiaxed microstructure with a grain size of 1 to 2 μm was obtained.

The increase in deformation temperature resulted in a lower dislocation density as shown in Figure 6(a) for the sample deformed at 980 °C. While, a few equiaxed

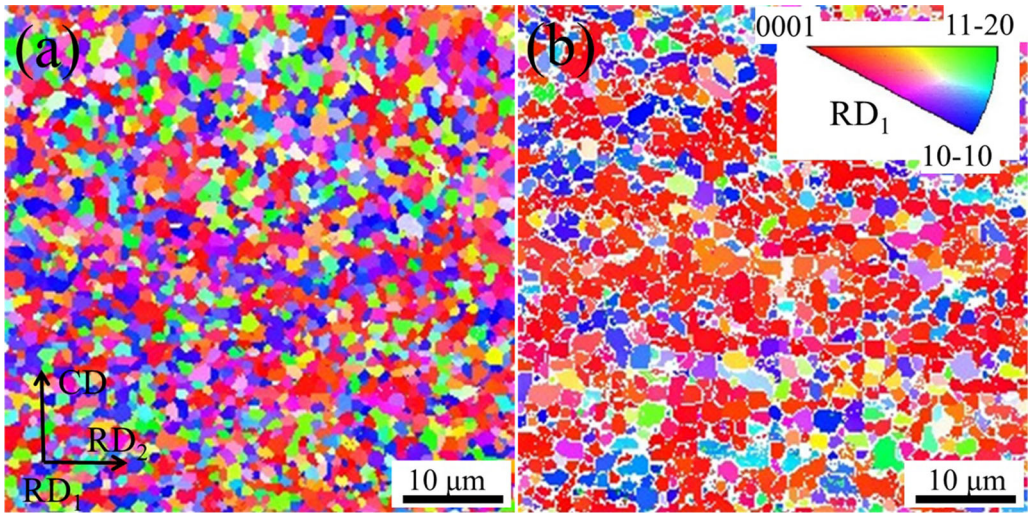

Fig. 4—EBSD orientation maps of the Ti60 alloy after compression at 900 °C (*a*) and 980 °C (*b*) at height reductions of 70 pct.

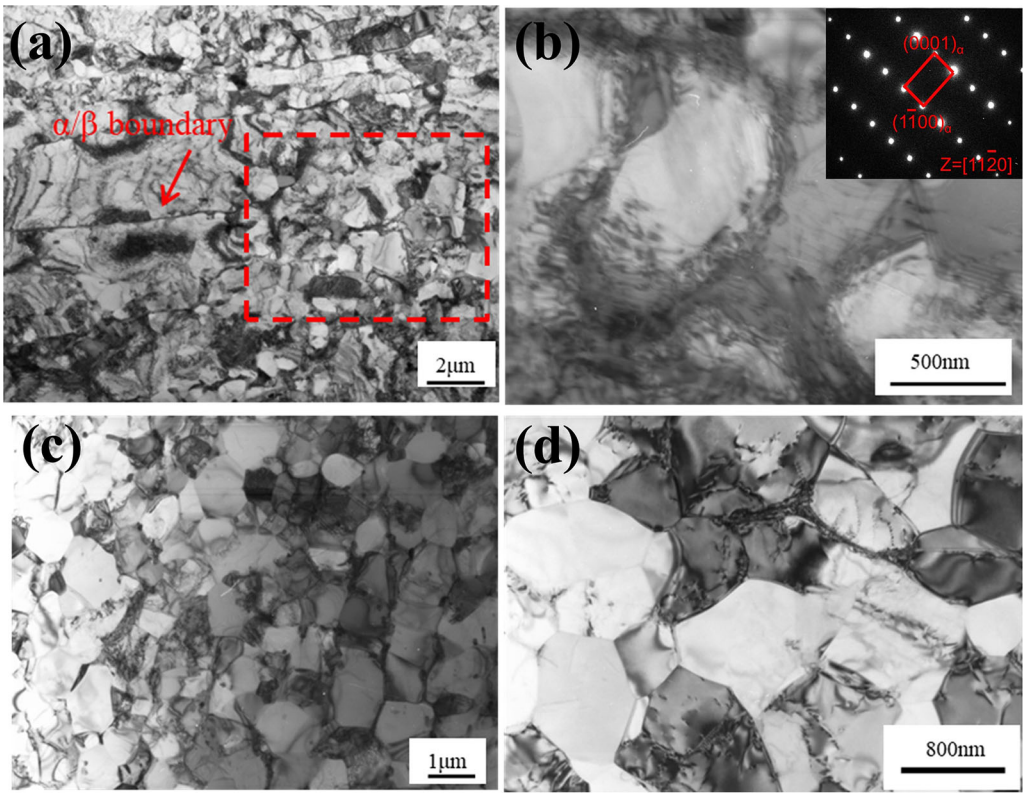

Fig. 5—TEM bright field images of Ti60 alloy with a height reduction of (*a*) and (*b*) 25 pct, (*c*) 50 pct, and (*d*) 70 pct by compression at 900 °C.

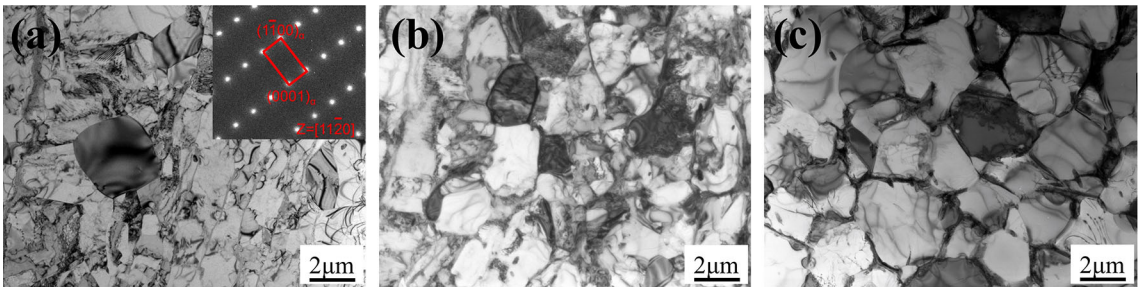

Fig. 6—TEM bright field images of Ti60 alloy with the height reduction of (*a*) 25 pct, (*b*) 50 pct, and (*c*) 70 pct by compression at 980 °C.

subgrains/grains with irregular shapes had already formed in the α laths after 25 pct height reduction. After height reduction of 50 pct at 980 °C (Figure 6(b)), the α laths became completely equiaxed with a mean α grain size of 3 μm. A further increase in the deformation strain to the height reduction of 70 pct (Figure 6(c)) led to a slight increase of the equiaxed grain size.

EBSD analysis also shows that a larger deformation imposed within the α lamellae in the material deformed at 900 °C than that deformed at 980 °C. The orientation variation of the undeformed lamellar structures is always within 2 deg, as the angular resolution of EBSD.[24] The present representative result for orientation variants analysis were selected by two deformed α laths with similar orientation. As shown in Figure 7, the magnitude of the orientation gradient decreased with the increasing deformation temperature, where the misorientation was ~ 1.3 and 0.65 deg μm^{-1} in a grain deformed at 900 °C and a grain deformed at 980 °C, respectively. As a result, deformation in the β phase, and the rotation of the α lamellae, become much more marked with increasing deformation temperature.

Altogether, a greater internal deformation of the α lath was accommodated at 900 °C than at 980 °C. At 900 °C, the dislocation density and variation of orientation within the α lamellae dramatically increased in the initial stage of deformation. As the strain increased, the subgrains were produced (see Figure 5). Meanwhile, a steep orientation gradient leads to highly misoriented subgrains during subgrain growth. The potential recrystallization nucleus would be formed when this misorientation reaches that of a high-angle grain boundary. Those features of the dynamic globularization process in the α phase at 900 °C were typical of continuous

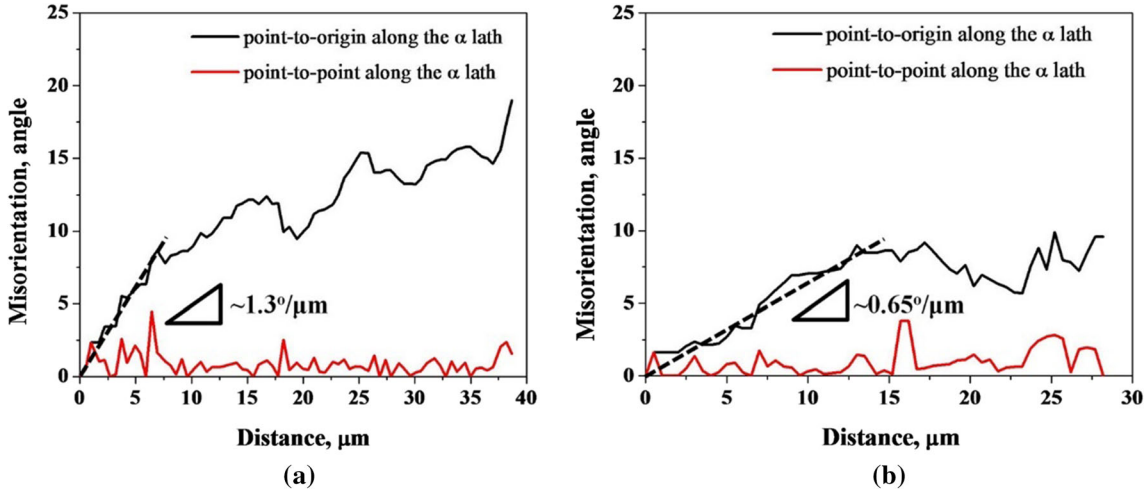

Fig. 7—Typical line scans from EBSD maps in Fig. 8 showing the variation in a grain of the material deformed at (*a*) 900 °C and (*b*) 980 °C. (Note: (a) and (b) correspond to grains A and B, respectively and the arrows in Fig. 8 indicate the line scan direction.).

dynamic recrystallization, which led to the formation of fine grains with random orientations. In addition, some fragmented grains with random orientations could be produced in local shear bands and colony boundaries (Zones I and II) as shown in Figure 8. Therefore, a fine and weak textured microstructure was obtained at 900 °C after globularization.

The lesser degree of internal deformation of the α lath at 980 °C may be associated with the greater contribution of the α lamellae rotation and of β deformation to the accommodation of the imposed strain. The dislocation density and misorientation within the α lamellae increased slightly in the initial stage of deformation. As shown in Figure 6, coarse subgrains/grains with sizes almost equal to the width of the original α lath were produced with the strain. The globularization process was associated primarily with the boundary-splitting mechanism, as noted by Weiss *et al.*[11]. Such a misorientation of the subgrain boundary would increase when it grows in an orientation gradient. However, the neighboring β phase hinders the growth of the α grain during deformation. As a consequence, equiaxed α grains whose orientations are greatly changed could not be produced in great number during globularization, although some high-angle α/α boundaries may also evolve from recovery, recrystallization, or shearing. Thus, this globularization process does not create a large number of new orientations, as observed in previous works.[8] The α phase always retains a similar orientation, or at least a common *c*-axis, after globularization as shown in Zone III of Figure 8(b).

It is important to note that the slip activity and the morphological features are also related to the crystallographic orientation. In this work, the main texture component of the original material is ⟨0001⟩//CD fiber texture, and the Schmid factor of the pyramidal ⟨*a* + *c*⟩ system slip for grains with this texture component is large. A co-activation of various slip modes would be reasonably expected in the initial stage of the deformation, although the preferential system slip is prismatic ⟨*a*⟩. A large orientation change can develop when neighboring volumes of a grain deform on different slip systems and rotate to different end orientations. Additionally, if the plane of α lamellae was nearly parallel to the deformation direction, the kinking would occur at the initial stage of deformation. Some equiaxed α grains with relatively random orientation could be generated in the local shear band and also reported elsewhere.[24] As already mentioned, the *c*-axis of the transformed α lamellae is near parallel to its broad face. Thus, the angle between the broad face of α lamella and the stress direction is always larger than the angle between the *c*-axis and the stress direction. One would expect that the mainly original ⟨0001⟩//CD fiber texture also promote the kinking, especially for a relatively low processing temperature[11,39] and more specifically at 900 °C for this work, which also some help to produce a homogenous microstructure.

V. CONCLUSION

The microstructure and crystallographic orientation evolution of Ti60 alloy with α lamellae structure were studied by compression testing during deformation at 900 °C and 980 °C. The globularization process converting the α lamellae into equiaxed α grains was different at 900 °C and 980 °C. At 900 °C, the globularization process is dominated by continuous dynamic recrystallization. A fine homogenous microstructure in terms of morphology and crystallographic orientation distribution is obtained after globularization. At 980 °C, the globularization process is controlled by the boundary-splitting mechanism. A coarse equiaxed microstructure with strong ⟨11-20⟩ fiber texture and macrozones is produced after globalization.

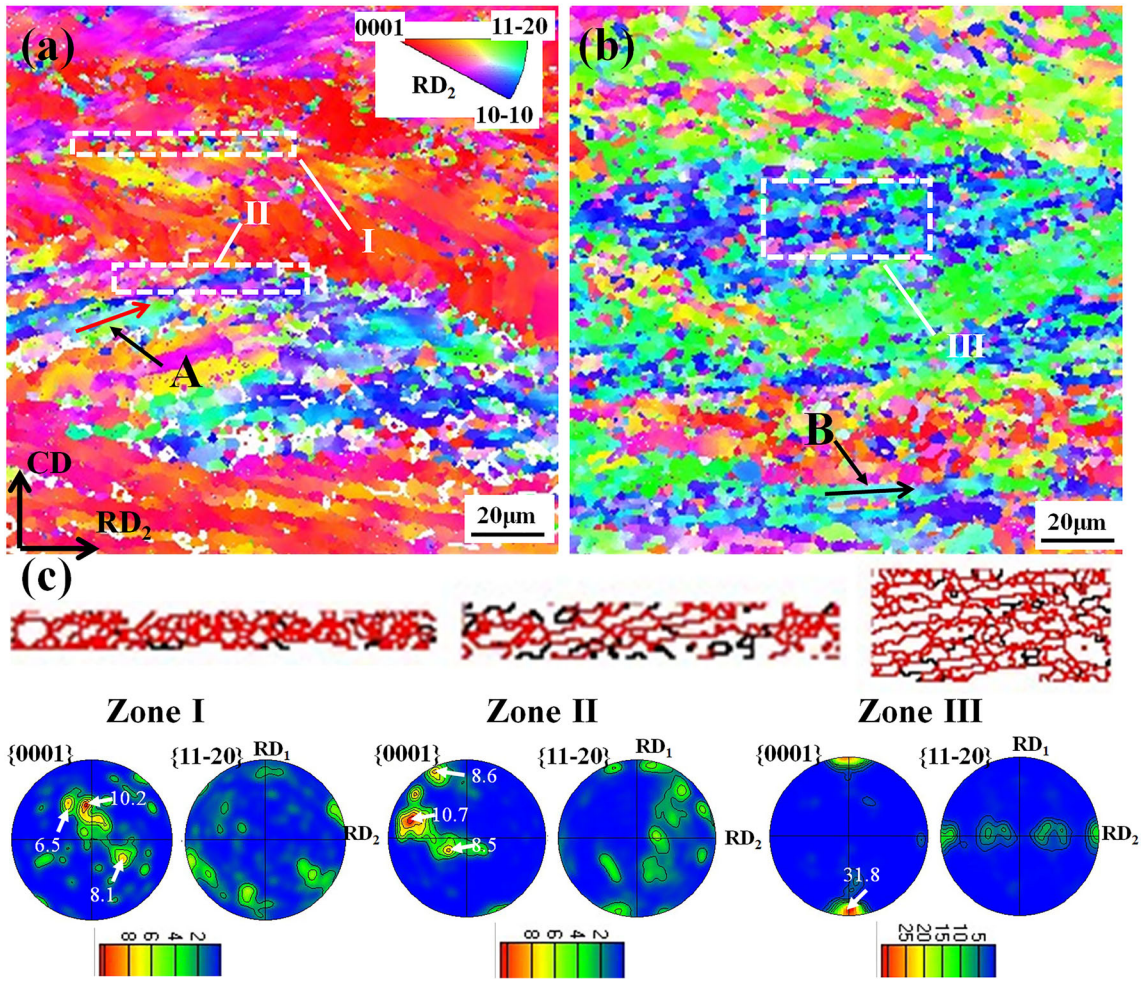

Fig. 8—IPF maps of the samples with height reduction of 25 pct at 900 °C (*a*) and 980 °C (*b*). Specific zones (I–III) as outlined by rectangles are analyzed in detail and their grain boundaries and local pole figure maps are shown in (*c*). Note that the high-angle boundaries ($\theta \geq 15$ deg) and the low-angle boundaries ($2 \leq \theta < 15$ deg) are depicted as red and black lines, respectively, in (c) (Color figure online).

ACKNOWLEDGMENTS

This work was supported by the National Science and Technology Major Project (J2019-VI-0005-0119), Youth Innovation Promotion Association CAS (No. 2020193), and CAS Project for Young Scientists in Basic Research (YSBR-025).

CONFLICT OF INTEREST

On behalf of all authors, the corresponding author states that there is no conflict of interest.

REFERENCES

1. L. Germain, N. Gey, M. Humbert, P. Bocher, and M. Jahazi: *Acta Mater.*, 2005, vol. 53(13), pp. 3535–43.
2. N. Gey, P. Bocher, E. Uta, L. Germain, and M. Humbert: *Acta Mater.*, 2012, vol. 60(6–7), pp. 2647–55.
3. Z.B. Zhao, Q.J. Wang, Q.M. Hu, J.R. Liu, B.B. Yu, and R. Yang: *Acta Mater.*, 2017, vol. 126, pp. 372–82.
4. P. Wanjara, M. Jahazi, H. Monajati, S. Yue, and J.P. Immarigeon: *Mater. Sci. Eng. A*, 2005, vol. 396(1–2), pp. 50–60.
5. P. Wanjara, M. Jahazi, H. Monajati, and S. Yue: *Mater. Sci. Eng. A*, 2006, vol. 416(1–2), pp. 300–11.
6. F. Heutling, D. Helm, M. Büscher, T. Witulski, M.L. Santaella, D. Eggermann, and M. Franzke: in *Proc. 13th World Conf. Titan.*, Wiley, 2016, pp. 1875–80.
7. J.L.W. Warwick, N.G. Jones, I. Bantounas, M. Preuss, and D. Dye: *Acta Mater.*, 2013, vol. 61(5), pp. 1603–15.
8. L. Germain, N. Gey, M. Humbert, P. Vo, M. Jahazi, and P. Bocher: *Acta Mater.*, 2008, vol. 56(16), pp. 4298–4308.
9. S.V. Zherebtsov, G.A. Salishchev, R.M. Galeyev, O.R. Valiakhmetov, S.Y. Mironov, and S.L. Semiatin: *Scripta Mater.*, 2004, vol. 51(12), pp. 1147–51.
10. J. Luo, J. Gao, L. Li, and M.Q. Li: *J. Alloys Compd.*, 2016, vol. 667, pp. 44–52.
11. I. Weiss, F.H. Froes, D. Eylon, and G.E. Welsch: *Metall Mater. Trans. A*, 1986, vol. 17A(11), pp. 1935–47.
12. S. Zherebtsov, M. Murzinova, G. Salishchev, and S.L. Semiatin: *Acta Mater.*, 2011, vol. 59(10), pp. 4138–50.
13. G.C. Obasi, S. Birosca, J. Quinta da Fonseca, and M. Preuss: *Acta Mater.*, 2012, vol. 60(3), pp. 1048–58.
14. M.G. Glavicic, B.B. Bartha, S.K. Jha, and C.J. Szczepanski: *Mater Sci. Eng. A*, 2009, vol. 513–514, pp. 325–28.

15. Y. Ito, H. Takamatsu, and K. Kinoshita: in *Proc. 13th World Conf. Titan.*, Wiley, 2016, pp. 885–88.
16. I. Bantounas, T.C. Lindley, D. Rugg, and D. Dye: *Acta Mater.*, 2007, vol. 55(16), pp. 5655–65.
17. A.L. Pilchak: *Scripta Mater.*, 2013, vol. 68(5), pp. 277–80.
18. J. Qiu, Y. Ma, J. Lei, Y. Liu, A. Huang, D. Rugg, and R. Yang: *Metall Mater. Trans. A*, 2014, vol. 45A(13), pp. 6075–87.
19. E. Uta, N. Gey, P. Bocher, M. Humbert, and J. Gilgert: *J. Microsc.*, 2009, vol. 233(3), pp. 451–59.
20. B. Poorganji, M. Yamaguchi, Y. Itsumi, K. Matsumoto, T. Tanaka, Y. Asa, G. Miyamoto, and T. Furuhara: *Scripta Mater.*, 2009, vol. 61, pp. 419–22.
21. G. Zheng, X. Mao, B. Tang, and Y. Zhang: *J. Alloys Compd.*, 2020, vol. 831, p. 154750.
22. T. Furuhara, B. Poorganji, H. Abe, and T. Maki: *JOM*, 2007, vol. 59(1), pp. 64–67.
23. L. Li, J. Luo, J.J. Yan, and M.Q. Li: *J. Alloys Compd.*, 2015, vol. 622, pp. 174–83.
24. S. Mironov, M. Murzinova, S. Zherebtsov, G.A. Salishchev, and S.L. Semiatin: *Acta Mater.*, 2009, vol. 57(8), pp. 2470–81.
25. M. Klimova, S. Zherebtsov, G. Salishchev, and S.L. Semiatin: *Mater Sci. Eng. A*, 2015, vol. 645, pp. 292–97.
26. H. Li, D.E. Mason, T.R. Bieler, C.J. Boehlert, and M.A. Crimp: *Acta Mater.*, 2013, vol. 61(20), pp. 7555–67.
27. H. Li, D.E. Mason, Y. Yang, T.R. Bieler, M.A. Crimp, and C.J. Boehlert: *Philos. Mag.*, 2013, vol. 93(21), pp. 2875–95.
28. M. Battaini, E.V. Pereloma, and C.H.J. Davies: *Metall. Mater. Trans. A*, 2007, vol. 38A(2), pp. 276–85.
29. Y.N. Wang and J.C. Huang: *Mater. Chem. Phys.*, 2003, vol. 81(1), pp. 11–26.
30. M.H. Yoo: *Metall. Mater. Trans. A*, 1981, vol. 12A(3), pp. 409–18.
31. Y.B. Chun and S.K. Hwang: *Acta Mater.*, 2008, vol. 56(3), pp. 369–79.
32. D.G. Leo Prakash, P. Honniball, D. Rugg, P.J. Withers, J. Quinta da Fonseca, and M. Preuss: *Acta Mater.*, 2013, vol. 61(9), pp. 3200–13.
33. N. Li, Z.B. Zhao, S.X. Zhu, T.Y. Zhou, Q.J. Wang, H. Sun, and Y.H. Liu: *Mater. Lett.*, 2021, vol. 288, p. 129363.
34. J.R. Bingert, T.A. Mason, G.C. Kaschner, G.T. Gray, and P.J. Maudlin: *Metall. Mater. Trans. A*, 2002, vol. 33A(3), pp. 955–63.
35. S. Zherebtsov, G. Salishchev, and S. Lee Semiatin: *Philos. Mag. Lett.*, 2010, vol. 90(12), pp. 903–14.
36. D. Bhattacharyya, G.B. Viswanathan, R. Denkenberger, D. Furrer, and H.L. Fraser: *Acta Mater.*, 2003, vol. 51(16), pp. 4679–91.
37. T. Furuhara, J.M. Howe, and H.I. Aaronson: *Acta Mater.*, 1991, vol. 39(11), pp. 2873–86.
38. D. Qiu, M.X. Zhang, P.M. Kelly, and T. Furuhara: *Acta Mater.*, 2014, vol. 67, pp. 373–82.
39. D. Banerjee, A.L. Pilchak, and J.C. Williams: *Mater. Sci. Forum*, 2012, vol. 710, pp. 66–84.